HHS Public Access

Author manuscript

Microcirculation. Author manuscript; available in PMC 2016 April 01.

Published in final edited form as:

Microcirculation. 2015 April ; 22(3): 204–218. doi:10.1111/micc.12195.

Robust and fragile aspects of cortical blood flow in relation to the underlying angioarchitecture

Andy Y. Shih[#1], **Charlotta Rühlmann**[#2], **Pablo Blinder**[3], **Anna Devor**[4], **Patrick J. Drew**[5], **Beth Friedman**[6], **Per M. Knutsen**[2], **Patrick D. Lyden**[7], **Celine Mateo**[2], **Lisa Mellander**[2], **Nozomi Nishimura**[8], **Chris B. Schaffer**[8], **Philbert S. Tsai**[2], and **David Kleinfeld**[2,9]

[1]Department of Neurosciences, Medical University of South Carolina, Charleston, SC

[2]Department of Physics, University of California at San Diego, La Jolla, CA

[3]Department of Neurobiology, Tel Aviv University, Tel Aviv, Israel

[4]Department of Neurosciences, University of California School of Medicine, La Jolla, CA

[5]Department of Engineering Science and Mechanics, Pennsylvania State University, University Park, PA

[6]Department of Pharmacology, University of California School of Medicine, La Jolla, CA

[7]Department of Neurology, Cedars-Sinai Hospital, Los Angeles, CA

[8]Department of Biomedical Engineering, Cornell University, Ithaca, NY

[9]Section of Neurobiology, University of California, La Jolla, CA

[#] These authors contributed equally to this work.

Abstract

We review the organizational principles of the cortical vasculature and the underlying patterns of blood flow under normal conditions and in response to occlusion of single vessels. The cortex is sourced by a two-dimensional network of pial arterioles that connects to a three-dimensional network of subsurface microvessels in close proximity to neurons and glia. Blood flow within the surface and subsurface networks is largely insensitive to occlusion of a single vessel within either network. However, the penetrating arterioles that connect the pial network to the subsurface network are bottlenecks to flow; occlusion of even a single penetrating arteriole results in the death of a 500 μm diameter cylinder of cortical tissue despite the potential for collateral flow through microvessels. This pattern of flow is consistent with that calculated from a full reconstruction of the angioarchitecture. Conceptually, collateral flow is insufficient to compensate for the occlusion of a penetrating arteriole because penetrating venules act as shunts of blood through collaterals. Future directions that stem from the analysis of the angioarchitecture concern cellular-level issues, in particular the regulation of blood flow within the subsurface microvascular network, and system-level issues, in particular the role of penetrating arteriole occlusions in human cognitive impairment.

Correspondence: David Kleinfeld, Ph. D. Department of Physics University of California 9500 Gilman Drive La Jolla, CA 92093-0374 dk@physics.ucsd.edu.

Keywords

Pial vessels; penetrating vessels; microvessels; imaging; rodent

The vasculature of the brain is tasked with the immense role of nurturing some one-hundred thousand energy-hungry neurons for every microliter of cortical tissue. To do so, it relies on a uniquely organized topology that leaves no portion of tissue without perfusion, with every neuron lying within fifteen micrometers of a brain capillary [1]. Here, we review a body of work on understanding the structure and function of the cortical vasculature, with ideas relating these discoveries on the rodent vasculature to human physiology. Our presentation is based on a lecture at the 2014 Microcirculatory Society President's Symposium. In keeping with the focused nature of that presentation, there is no pretense of historical perspective nor encyclopedic review. Further, we have stripped the presentation of a discussion of technical developments that fueled these results; these are reviewed elsewhere [2-6].

What are the issues that make the study of brain vasculature both interesting and challenging? First, we suggest, there is the need for dynamic allocation of resources, *i.e.*, oxygen and nutriments, to brain cells. Blood is a limited resource, yet neural function depends on adequate flow. In particular, the pioneering work of Fox and Raichle [7] suggest that there is simply not enough blood to go around if all areas of the cortex were activated at once. To achieve this dynamic allocation, there is a coupling of blood flow with neuronal energetics and electrical activity [8-10]. The correlation is imperfect, with poorly understood relationships between flow, oxygenation, and neural activity [11]. Nonetheless, this coupling permits functional magnetic resonance imaging [12, 13] (fMRI) to be used to study brain function in humans, a necessity for addressing many issues in cognition. Next, neuronal and vascular development appear to follow a similar plan and are linked by common genomic markers that control the fate of both systems [14]. Finally, there is strong if only partially understood coupling between neuronal and vascular dysfunction [15]. In particular, vascular disease leads to neurological decline and diminished cognition and memory [16].

Cortical Angioarchitecture is Organized into Three Tiers

A single microliter of cortex holds nearly one meter of total vascular length [17]. Though densely packed, the vasculature can be organized into three distinct topological tiers that blood must pass through to supply the brain. These tiers consist of the pial surface arteriole and venule networks, the subsurface microvascular network, and the penetrating arterioles and venules that bridge the surface and subsurface networks (Figure 1).

In the first tier, a plexus of arteries and arterioles that collectively occupy the territory of the middle cerebral artery (MCA) covers the surface of about half of neocortex [18, 19]. The MCA originates from the circle of Willis at the base of the brain and extends over the cortical mantle as a network of two-dimensional loops. These loops are formed when branches of the MCA connect through anastomoses [20, 21]. Penetrating arterioles branch from the surface arterial network and plunge perpendicularly into cortex [22, 23]. The vast majority of penetrating arterioles are singular offshoots that do not branch further on the pial

surface before entering the brain [21]. This is an important geometrical feature that ensures each penetrating arteriole can be sourced by two potential inputs within a vascular loop. As penetrating arterioles descend into the cortex, they gradually ramify into pre-capillary arterioles that, in turn, feed into the subsurface microvascular network.

The microvascular network comprises a three-dimensional network [17]. All cerebral blood flow must pass through this network in order to exit the brain, as there are no direct arteriole to venule anastomoses in the healthy brain. The density of the capillaries is largely homogeneous along varying depths of the cortex, even though the density and composition of cells varies greatly over the cortical thickness [1, 24].

Finally, blood exits the cortex through a venular system that is similar to the arterial system. Penetrating venules receive blood from post-capillary venules that drain the subsurface microvascular network and run perpendicular to the brain surface [25]. After exiting the parenchyma, blood flows through a tree-like venular surface network and finally drains into the central sinus [18, 19].

Robust blood flow through the pial network

A detailed analysis of the pial angioarchitecture was created from images of surface vessels that were filled with a gel linked to a fluorescent dye [21]. We mapped the location of all vessels and found that an interconnected backbone of vessels spans the full territory of the MCA (black overlay on green, Figure 2a). This angioarchitecture provides multiple paths for the supply of blood to any penetrating arteriole. This implies that blood flow can be redistributed to areas of need from areas of excess; such a redistribution could not occur with a tree-like branching pattern.

Does the observed architecture support the redistribution of blood over the cortical mantle in response to a “hot spot” of neuronal activation? To test this possibility, we stimulated the forepaw of an anesthetized animal so that the contrast in activity between the core region of somatotopic activation and the surrounding regions is particularly large (left and middle panels of Figure 2b). Optical imaging with *in vivo* two-photon laser scanning microscopy (TPLSM) [26, 27] enables lumen diameter to be observed. We found that there is a local dilation of arterioles at the center of the electrophysiological response [28]. Yet as one moves away from the center the vascular response is dominated by an average constriction rather than dilation (middle and right panels of Figure 2b). This center-surround effect suggests that the network of arterioles on the pial surface shunts blood flow from inactive to active brain areas through active dilation and constriction.

These above findings indicate that vascular tone has local control in addition to pial-wide control during functional hyperemia [29]. The mechanism for the spatiotemporal coordination of arteriolar reactivity is incompletely understood, but it is likely to involve conduction of a parenchymal response to the pial network through vascular endothelial gap junctions [30] with a ~ 2 mm electrotonic length along the endothelial cells that form a vessel [31]. The endothelial response result in either dilation or constriction by engaging distinct myoendothelial signaling cascades [32]. Since a multitude of penetrating arterioles exist along a single branch of the MCA, different regions of cortex can be seeded with either

dilatory or constrictive signals and, in principle, this can result in a center-surround shift in blood flow.

Beyond issues of dynamic reallocation of blood, the high interconnectivity of the surface network should make the distribution of blood relatively insensitive to blockages of a single surface vessel. To test this hypothesis, we used TPLSM to track the speed of red blood cells (RBCs) [27] and used focused excitation of a photosensitizer, transiently introduced into the blood stream, to form a clot at a vessel of interest [33] (Figure 2c). Immediately after the clot is formed, we find a reversal in the direction of flow of one of the pair of proximal downstream vessels [33], such that the magnitude of the flow remains roughly equal even though the direction of flow has flipped. Thus the ability of the surface network to source blood to neocortex is unaffected by a single localized defect.

Before moving on, we consider the role of the pial arterioles in distributing blood to the penetrating arterioles during a transient blockage of the MCA, a model of stroke [34, 35]. We find that the available blood is homogeneously distributed to all penetrating arterioles as flow is diminished [36], as opposed to creating patches of cortex with flow versus no-flow. Thus the maintenance of flow homogeneity in penetrating arterioles as a population also relied upon the ability of the pial network to redistribute blood, which also involved reversals of flow in anterior cerebral artery collaterals as well as in smaller collaterals between major MCA branches (Figure 2a). In fact, recent studies show that stroke severity can be predicted by the extent of vascular collateralization from animal to animal [37].

Dynamic changes in pial vessel diameter are modest in extent

We observed changes of 5 % in the diameter of pial vessels in anesthetized animals [28, 38] (Figure 2b). This number is small, suggesting that regulation makes only a modest difference in vasodynamics. Does the fractional change hold up in awake animals? We address this issue in awake, head-fixed mice in which vasodynamics are measured through a transcranial window [39] (Figure 3a). Sensory simulation, in this case an air puff to the vibrissae, leads to changes in the diameter of the pial arterioles of at most 40 % (Figure 3b). Interestingly, there is also spontaneous vasodilation, referred to as vasomotor events [40], whose maximal dilation is similar in size [39] (Figure 3c). These spontaneous events occur over time scales of seconds to tens of seconds and involve changes in vascular smooth muscle calcium signaling and other components that may control vascular tone [41]. The essential issue is that changes in diameter of pial vessels are modest in extent in comparison with the many-fold increases that are seen in the vasculature of peripheral muscles through capillary recruitment [42].

It is noteworthy that the magnitude of arteriolar dilations measured *in vivo* rarely exceeds a 40 % increase from baseline. This apparent limitation exists regardless if an animal is awake or under anesthesia, or if the dilation is evoked by sensory input or part of an ongoing vasomotor oscillation. Exogenous manipulations, such as isoflurane inhalation [43] or shock [44], can drive an increase in the diameter of arterioles in excess of 40%, but under physiological conditions, a homeostatic mechanism may exist to prevent over-distention of the arteriole wall.

Subsurface microvessels show both stimulus-activated and spontaneous changes in the speed and flux of RBCs [27]. Interestingly, the flow of RBCs rarely transitions from moving to stalled [27, 45]. All told, since blood in all arterioles and all capillaries is flowing at all times under normal conditions, there is no reserve of vascular volume to be filled by increased flow in upstream arterioles. This may ensure that the brain does not swell beyond the capacity of the intracranial space. Further, the consistency of flow and the observation that changes in flow are not too great suggests that a linear analysis of flow based on a fixed angioarchitecture should have utility in predicting flow patterns.

Robust aspects of subsurface blood flow

The reconstruction of the microvasculature across many microliters of tissue (Figure 1) may be analyzed to determine the topology of the subsurface microvasculature (Figure 4a). Like the pial vasculature, we observe loops, albeit composed of a greater number of branches than those on the surface (Figure 4b). This finding suggests that flow in the subsurface vasculature should also be relatively immune to occlusion to a single vessel. We used a sensitizer-free, nonlinear optical technique to injure the endothelium and trigger clotting in a targeted subsurface vessel [46]; nonlinear interactions are required so that light is absorbed not above or below the targeted vessel. We observed highly reduced flow in the proximal downstream vessel, as opposed to the immediate recovery for surface loops (*cf* Figure 4c and 2c), yet there was substantial recovery by three vessel branches downstream (Figure 4c). Further, histological analysis of the tissue indicates that there is essentially no neuronal damage in terms of markers of hypoxia or neuronal structure [46, 47]. We conclude that clots targeted to single vessels in either surface or subsurface networks cause negligible ischemia or damage to neurons. This occurs as a consequence of redundant flow pathways.

Penetrating vessels are a fragile link in the sourcing of blood

Penetrating vessels deliver blood from the surface network to subsurface microvasculature. They are interconnected by way of the dense microvasculature (Figures 1 and 4a), but do not connect with each other through direct subsurface collaterals [17] (Figure 5a). Thus it is not obvious whether the loss of flow to a penetrating vessel would terminate all flow to the tissue volume perfused by the vessel. On the one hand, penetrating vessels deliver, on average, a median flux of blood into the brain that is seventy-times the mean flux through an individual microvessel [47]. Yet the multitude of microvessels suggests that collateral flow could compensate for the absence of a penetrating vessel. To observe what actually occurs for this critical case, we made use of our previous technique of blocking flow in pial vessels (Figure 2c), but this time directed at the entry point where a penetrating arteriole plunges into cortex (Figure 5a). We measured the change in the speed of RBCs in downstream vessels as a function of lateral distance for the site of occlusion (Figure 5b). We found that the speed, and thus flux of RBCs, goes to zero in downstream vessels that lie distal to the occlusion and does not fully recover until a radius of about 250 micrometers from the occluded penetrating arteriole [23, 48]. Thus the loss of flow to a single penetrating arteriole leads to an acute loss of perfusion in a columnar region that spans approximately 500 micrometers in diameter.

Biomedical Consequences of the Loss of One Penetrating Arteriole

What are the chronic consequences of the loss of perfusion from a single penetrating vessel? A simple but telling measurement in the rodent is to probe for ischemic spreading depression, *i.e.*, a front of potassium and glutamate that further contributes to stroke damage [49]. These measurements make use of a fluorescent indicator of intracellular calcium as a proxy for electrical depolarization [50] (Figure 6a), yet are qualitative in the sense that the onset time of spreading depression is unpredictable. Nonetheless, in a significant number of cases we see a slowly propagating front of depolarization followed by inactivity (Figure 6b).

A gold standard of neurological damage is the presence of an infarct [51]. In subacute stages of stroke, the infarcted region is filled with phagocytic inflammatory cells. As such, we repeated the procedure of occluding a single penetrating vessel in mice that expressed green fluorescent protein (GFP) in microglia/monocytes and, further, we used transcranial illumination to obviate the possibility that a chronic, cranial window compromising the data [52] (Figure 6c). When the animals are sacrificed six days later, we observe a cylindrical region of infarcted tissue, highlighted by microglia and monocytes that have swarmed to the region [52] (Figure 6d). The diameter of the cylinder is approximately 500 micrometers, the same as the region of acute loss of flow.

The microinfarcts caused by occlusion to a single penetrating arteriole (Figure 6d) are several orders of magnitude smaller than the infarcts seen in experimental strokes caused by occlusion of the MCA [34]. Therefore, it stands to question whether such small lesions could generate a perceptible deficit in brain function. We distilled the behavioral deficit imparted by a single microinfarct [47] using a refined version of the gap-crossing task of Hutson and Masterton [53]. Here a rat uses a single vibrissa to sense, in the dark, the presence or absence of a platform that is across a gap. The occlusion was strategically generated in a penetrating arteriole that was centered in a cortical column that receives input from that single vibrissa. We found that the microinfarct led to an altered decision on whether to navigate the gap, implying that the rat lost the capability to make a specific sensorimotor decision [47]. Related studies in mice suggest that microinfarcts exert a diaschisis that impairs neural excitability well outside the region of tissue infarction [54].

Calculated Versus Measured Flow After an Occlusion

The complete reconstruction of microliter volumes of neocortex (Figure 1) allows us to calculate the expected change in flow after occlusion of a vessel and compare the calculated change against measured values. This serves as a test of self-consistency between two independent approaches, *i.e.*, flow measurements versus computations based on structural measurements. Each vascular junction is connected to three others by vessels of known median radius and length (Figure 7a). A single number, the resistance of the vessel to the flow of RBCs, characterizes the vessel and is based on the formula of Pries and Secomb [55] (Figure 7b; dashed line is the curve expected for water). We then apply Kirchhoff's law to each junction and use known values for the inlet pressure to surface arterioles to calculate the flux through every vessel [17]. Our first numerical experiment is to determine the volume of cortex that receives the major fraction of perfusion from a given penetrating

arteriole. We find a linear relation between the calculated volume and the flux of RBCs through the penetrating arteriole over two-orders of magnitude of flux (Figure 7c). The observed linearity is consistent with the fully connected nature of the subsurface microvasculature, while the scatter in the calculated values reflects the random pattern of subsurface connections (Figure 4a,b). Critically, the volume of a cyst formed by blockage of a single penetrating vessel (Figure 6d) coincides with the volume of perfusion (Figure 7d). This establishes the notion of a territory of perfusion for each penetrating arteriole. These territories are unrelated to the columnar organization of neuronal afferents [17].

Our second numerical experiment addresses the catastrophic loss of perfusion in the vicinity of an occluded penetrating arteriole. We calculate the change in RBC flux, and accompanying speed, in microvessels downstream of the occluded arteriole in terms of branch number (Figure 7e). There are no free parameters in the calculation. As an average over all penetrating vessels in all reconstructions, we observe that the median value of the speed recovers to half of the pre-occlusion value by six downstream branches [17] (D6 in Figure 7f). These calculated values are compared with measurements of the decrement in pre-occlusion speed as a function of the branch order away from an occluded penetrating vessel [48] (*cf* yellow/green and red diamonds in Figure 7e). The midpoint of the recovery matches and the overall shape of the curves are consistent; the mismatch for branches D1 to D4 occurs since the calculated speed cannot go to zero in our linear analysis. We argue that this analysis supports the role of linear analysis for modeling blood flow.

Insight into the lack of collateral flow

The above numerical analysis establishes self-consistency, yet gives little insight into the reason why collateral flow through microvessels does not counter the loss of perfusion through the penetrating arteriole. Motivation for a simplified model comes from the anatomical drawings of retinal vasculature by Snodderly, Weinhaus and Choi [56], which shows that the blood supply to a disk of microvasculature is sourced and sunk by radial, alternating penetrating arterioles and penetrating venules. We thus consider a two-dimensional rhombic lattice, with the observed ratio of two penetrating venules to one penetrating arteriole, as a model of neocortical vasculature [17] (Figure 8a). We take penetrating arterioles as ideal pressure sources, penetrating venules as grounds, and replace individual microvessels with the Thévenin resistance between distant junctions; this ignores the resistance of penetrating vessels, which is half that of the Thévenin resistance. Blockage of a penetrating arteriole leads to an unperfused hexagon of tissue as flow through the microvascular network toward the region of the occlusion is shunted through the penetrating venules (Figure 8b). Similarly, blockage of a penetrating venule leads to an unperfused hexagon of tissue as the removal of a sink raises the impedance of flow into the region (Figure 8c). This model highlights why blockage of any penetrating vessel leads to an infarct through a lack of flow, with good agreement between theory and experiment especially considering the brutal nature of approximations (Figure 8b,c). The inability for the vasculature to compensate for flow loss to the regions of an occluded penetrating vessel is a key fragility in an otherwise remarkably robust system [23, 48].

Synopsis

All told, the picture that emerges is one of a highly interconnected surface vasculature that forms a two-dimensional network and is a robust source of blood to the penetrating arterioles (Figure 2). The subsurface microvasculature forms a three-dimensional network that is fully connected and forms a robust source of nutriment to the neurons and glia throughout neocortex (Figure 4). However, flow in the penetrating arterioles and venules that traffic between the surface and subsurface networks is fragile (Figure 5a), in the sense that blockage of one vessels leads to a break in the supply chain and neuronal death throughout a cylinder of cortex (Figures 5b and 6d).

Next Steps

Open issues remain at the level of basic physiology and biofluidmechanics as well as in biomedicine. With regard to basic issues, none is greater than the means by which the nervous system controls vascular tone.

Resting-state fluctuation in blood oxygenation

We consider the issue of vasomotion [39, 40] (Figure 4) and the potential connection to the resting state signal in BOLD fMRI [57]. The resting state signal is a roughly 0.1 Hz oscillation in the blood volume and/or the oxygenation state of hemoglobin in the blood that, further, is correlated in time between regions of cortex with similar function [58, 59]. For example, the areas of motor cortex that control motion of the index finger in each hand would have correlated BOLD signals. There is evidence for callosal inputs that communicate low frequency electrical activity between such areas [60]. Thus we conjecture that low frequency electrical activity entrains the intrinsic oscillators in smooth muscle that drive vasomotion [61, 62], and that tissue oxygenation is slaved to vasomotion, as the origin of the synchronous activity in the resting state. Evidence to support this conjecture represents work in progress [63]. In particular, it remains unclear if vasomotion drives tissue oxygenation or, rather, that vasomotion is slaved to tissue oxygenation and renders our conjecture false.

Pericytes as control elements to flow through the subsurface microvasculature

The flux of blood through the microvessels in a function of the resistance of the network and the pressure difference between pial arterioles and venules. The resistance of a microvessel is an exquisitely sharp function of its diameter (Figure 7b) since the size of the vessel is close to that of RBCs [55]. This suggests that significant changes in resistance will accompany sub-micrometer changes in diameter. Both smooth muscle and pericytes are cell types that could act as control elements as these cells ensheath vessels and contain contractile filaments although pericytes are unique to subsurface microvessels [64]. Evidence from *in vitro* studies that include demonstrations of pericyte contraction in response to electrical stimulation [65], neurotransmitters [65-67], and simulated ischemia [66] support a role for the control of microvessel diameter through the activation of pericytes. However, there is contradictory data obtained in live animals concerning changes

in the diameter of microvessels that are ensheathed by a pericyte [66, 68]. A key difficulty is distinguishing pericytes from smooth muscle *in vivo*.

What molecular markers are available to highlight pericytes for guidance during *in vivo* measurements? Pericytes express the smooth muscle isoform of actin [69], which makes them difficult to distinguish from the smooth muscle of subsurface arterioles, although pericytes located on microvessels that lie midway between penetrating arterioles and venules may lack contractile elements [70]. Similarly, the proteoglycan NG2, which is often used as a marker for pericytes [71] (Figure 9), is also expressed in arteriolar smooth muscle. This data raises questions about the utility of a mouse line that links the expression of the proteoglycan NG2 to the fluorescent protein DsRed [72, 73] for studies on pericytes. The intermediate filament desmin, however, is expressed in arteriolar smooth muscle but not pericytes of the brain [69, 74] (Figure 9bd). In principal one can use an intersectional, dual-recombinase strategy [75] to form a transgenic animal that labels only pericytes. We provide an example two-step scheme (Figure 9e) that is based on an initial activation of fluorescent protein expression in the Ai3 reporter line [76] through breeding with the existing NG2::CreER^{TM} driver line [73]. The resulting bigenic progeny are then bred with a hypothetical desmin::Flp driver line to subtract fluorescent protein expression from arterial smooth muscle, while leaving pericyte expression intact.

Relation of microlesions to human disease

The lesions generated by the occlusion of single penetrating arterioles bear remarkable similarity in location and shape to microinfarcts seen in the aging human brain [47]. While most data supporting the existence of microinfarcts in humans comes from neuropathological studies [77] (Figure 10b), there is mounting evidence to suggest that these lesions can be detected and tracked during life using high-field MRI [78] (Figure 10b) and most recently clinical MRI [79]. Several groups have shown that vascular cognitive impairment is strongly correlated with an increased incidence of microinfarcts [16, 80-82]. Thus improved methods to detect microinfarcts by MRI are essential in the treatment of dementia, which must be identified before the onset of clinical symptoms. We suggest that rodent models of vascular cognitive impairment will be integral to the design of protocols for early detection through MRI imaging and mitigation of continued spread of dysfunction through pharmacological intervention [83].

A second and no less perilous form of microscopic lesion is the cerebral microbleed [84-87]. These are caused by rupture of microvessels, generating lesions that exist on a similar size scale as microinfarcts as seen with high-field MRI (Figure 10c). Microbleeds increase the likelihood of dementia, and like microinfarcts, their role in the pathogenesis of vascular cognitive impairment remains poorly understood. Microbleeds can be modeled in rodents through the use of nonlinear absorption of laser pulses to breach the vascular wall [46]. *In vivo* imaging has demonstrated the ability of microbleeds to compress surrounding tissue but, remarkably, this leads to minimal impact on neuronal structure and function [88, 89]. In light of clinical evidence for microbleeds in even middle-aged adults [86], it is imperative to pursue optically induced microinfarcts and microbleeds as experimental platforms to modeling their human counterparts in a controlled manner. It is especially relevant to pursue

models of lesions to white matter in rodents, given the prevalence of white matter lesions in the human brain [90].

Epilog

Continued progress toward our understanding of the neurovascular system will depend in part on the adoption of new tools. Studies on the logic of vasoactive transmitters will gain from the use of cell-based indicators of amine and peptide transmitters [91] and expanded use of structural and functional markers of vascular function [92]. The detection of relatively small changes in the diameter of microvessels will gain from the use of sub-diffraction imaging techniques [93]. Lastly, studies on biomedical issues that concern microlesions in white matter and the mechanisms of vascular dementia will gain from nonlinear optical techniques for deep imaging that exploit windows in the absorption spectrum of water at long wavelengths [94, 95].

Acknowledgements

The study on blood flow by Kleinfeld, Helmchen, Mitra and Denk (1998) that initiated this effort was motivated, in part, by a discussion with Thomas A. Woosley and Carl M. Rovainen in 1995. Our thinking on vascular dementia gained focus from conversations with Geerte J. Biessels, Sandra E. Black and Martin Dichgans. The Kleinfeld laboratory received support from the David and Lucile Packard Foundation (grant 99-8326), the National Institutes of Health (grants EB003832, MH72570, NS059832, OD006831/NS082097, and RR021907), and the National Science Foundation (grant 0455027). The Shih laboratory received support from the American Heart Association (grant 14GRNT20480366), the Dana Foundation, the National Institutes of Health (grants NS085402 and P20GM12345), and the South Carolina Clinical and Translational Institute (grant UL1TR000062).

References

1. Tsai PS, Kaufhold J, Blinder P, Friedman B, Drew P, Karten HJ, Lyden PD, Kleinfeld D. Correlations of neuronal and microvascular densities in murine cortex revealed by direct counting and colocalization of cell nuclei and microvessels. Journal of Neuroscience. 2009; 18:14553–14570. [PubMed: 19923289]
2. Kleinfeld, D.; Denk, W. Two-photon imaging of neocortical microcirculation. In: Yuste, R.; Lanni, F.; Konnerth, A., editors. Imaging Neurons: A Laboratory Manual. Cold Spring Harbor Laboratory Press; Cold Spring Harbor: 1999. p. 23.1-23.15.
3. Tsai, PS.; Kleinfeld, D. In vivo two-photon laser scanning microscopy with concurrent plasma-mediated ablation: Principles and hardware realization. In: Frostig, RD., editor. Methods for In Vivo Optical Imaging. 2nd edition. CRC Press; Boca Raton: 2009. p. 59-115.
4. Kleinfeld, D.; Mitra, PP. Applications of spectral methods in functional brain imaging. In: Yuste, R., editor. Imaging: A Laboratory Manual. Cold Spring Harbor Laboratory Press; New York: 2011. p. 12.1-12.7.
5. Shih AY, Mateo C, Drew PJ, Tsai PS, Kleinfeld D. A polished and reinforced thinned skull window for long-term imaging and optical manipulation of the mouse cortex. Journal of Visualized Experiments. 2012http://www.jove.com/video/3742
6. Shih AY, Driscoll JD, Drew PJ, Nishimura N, Schaffer CB, Kleinfeld D. Two-photon microscopy as a tool to study blood flow and neurovascular coupling in the rodent brain. Journal of Cerebral Blood Flow & Metabolism. 2012; 32:1277–1309. [PubMed: 22293983]
7. Fox PT, Raichle ME. Focal physiological uncoupling of cerebral blood flow and oxidative metabolism during somatosensory stimulation in human subjects. Proceedings of the National Academy of Sciences USA. 1986; 83:1140–1144.
8. Roy CS, Sherington CS. On the regulation of the blood supply of the brain. Journal of Physiology. 1890; 11:85–108.

9. Iadecola C, Nedergaard M. Glial regulation of the cerebral microvasculature. Nature Neuroscience. 2007; 10:1369–1376.
10. Attwell D, Buchan AM, Charpak S, Lauritzen M, MacVicar BA, Newman EA. Glial and neuronal control of brain blood flow. Nature. 2010; 468:232–43. [PubMed: 21068832]
11. Kleinfeld D, Blinder P, Drew PJ, Driscoll JD, Muller A, Tsai PS, Shih AY. A guide to delineate the logic of neurovascular signaling in the brain. Frontiers in Neuroenergetics. 2011; 1:1–9. [PubMed: 21559095]
12. Ogawa S, Lee T-M, Nayak AS, Glynn P. Oxygenation-sensitive contrast in magnetic resonance image of rodent brain at high fields. Magnetic Resonance in Medicine. 1990; 14:68–78. [PubMed: 2161986]
13. Logothetis NK, Wandell BA. Interpreting the BOLD signal. Annual Review Physiology. 2004; 66:735–769.
14. Carmeliet P, Tessier-Lavigne M. Common mechanisms of nerve and blood vessel wiring. Nature. 2005; 436:193–200. [PubMed: 16015319]
15. Girouard H, Iadecola C. Neurovascular coupling in the normal brain and in hypertension, stroke, and Alzheimer disease. Journal of Applied Physiology. 1985; 100:328–335. [PubMed: 16357086]
16. Gorelick PB, Scuteri A, Black SE, DeCarli C, Greenberg SM, Iadecola C, Launer LJ, Laurent S, Lopez OL, Nyenhuis D, Petersen RC, Schneider JA, Tzourio C, Arnett DK, Bennett DA, Chui HC, Higashida RT, Lindquist R, Nilsson PM, Roman GC, Sellke FW, Seshadri S. Vascular contributions to cognitive impairment and dementia: A statement for healthcare professionals from the American Heart Association/American Stroke Association. Stroke. 2011; 42:2672–713. [PubMed: 21778438]
17. Blinder* P, Tsai* PS, Kaufhold JP, Knutsen PM, Suhl H, Kleinfeld D. The murine cortical angiome: An interconnected vascular network with noncolumnar patterns of blood flow. Nature Neuroscience. 2013; 16:889–897.
18. Scremin, OU. Cerebral Vascular System. In: Paxinos, G., editor. The Rat Nervous System. Academic Press, Inc.; San Diego: 1995.
19. Mchedlishvili, G. Arterial Behavior and Blood Circulation in the Brain. Consultants Bureau; New York: 1963.
20. Coyle P, Jokelainen PT. Dorsal cerebral arterial collaterals of the rat. Anatomical Record. 1982; 203:397–404. [PubMed: 7137595]
21. Blinder* P, Shih* AY, Rafie CA, Kleinfeld D. Topological basis for the robust distribution of blood to rodent neocortex. Proceedings of the National Academy of Sciences USA. 2010; 107:12670–12675.
22. Bär T. The vascular system of the cerebral cortex. Advances in Anatomy, Embryology and Cell Biology. 1980; 59:1–62.
23. Nishimura N, Schaffer CB, Friedman B, Lyden PD, Kleinfeld D. Penetrating arterioles are a bottleneck in the perfusion of neocortex. Proceedings of the National Academy of Sciences USA. 2007; 104:365–370.
24. Weber B, Keller AL, Reichold J, Logothetis NK. The microvascular system of the striate and extrastriate visual cortex of the macaque. Cerebral Cortex. 2008; 18:2318–2330. [PubMed: 18222935]
25. Nguyen J, Nishimura N, Fetcho RN, Iadecola C, Schaffer CB. Occlusion of cortical ascending venules causes blood flow decreases, reversals in flow direction, and vessel dilation in upstream capillaries. Journal of Cerebral Blood Flow & Metabolism. 2011; 31:2243–2254. [PubMed: 21712834]
26. Svoboda K, Denk W, Kleinfeld D, Tank DW. *In vivo* dendritic calcium dynamics in neocortical pyramidal neurons. Nature. 1997; 385:161–165. [PubMed: 8990119]
27. Kleinfeld D, Mitra PP, Helmchen F, Denk W. Fluctuations and stimulus-induced changes in blood flow observed in individual capillaries in layers 2 through 4 of rat neocortex. Proceedings of the National Academy of Sciences USA. 1998; 95:15741–15746.
28. Devor A, Tian P, Nishimura N, Teng IC, Hillman EM, Narayanan SN, Ulbert I, Boas DA, Kleinfeld D, Dale AM. Suppressed neuronal activity and concurrent arteriolar vasoconstriction

may explain negative blood oxygenation level-dependent signaling. Journal of Neuroscience. 2007; 27:4452–4459. [PubMed: 17442830]

29. Hamel E. Perivascular nerves and the regulation of cerebrovascular tone. Journal of Applied Physiology. 2006; 100:1059–1064. [PubMed: 16467392]
30. Bagher P, Segal SS. Regulation of blood flow in the microcirculation: Role of conducted vasodilation. Acta Physiologica. 2011; 202:271–284. [PubMed: 21199397]
31. Segal SS, R. DB. Flow control among microvessels coordinated by intercellular conduction. Science. 1986; 234:868–870. [PubMed: 3775368]
32. Dietrich HH, Kajita Y, Dacey RGJ. Local and conducted vasomotor responses in isolated rat cerebral arterioles. American Journal of Physiology. 1996; 271:H1109–1116. [PubMed: 8853348]
33. Schaffer CB, Friedman B, Nishimura N, Schroeder LF, Tsai PS, Ebner FF, Lyden PD, Kleinfeld D. Two-photon imaging of cortical surface microvessels reveals a robust redistribution in blood flow after vascular occlusion. Public Library of Science: Biology. 2006; 4:258–270.
34. Zea Longa E, Weinstein PR, Carlson S, Cummins R. Reversible middle cerebral artery occlusion without craniectomy in rats. Stroke. 1989; 20:84–91. [PubMed: 2643202]
35. Memezawa H, Minamisawa H, Smith ML, Siesjo BK. Ischemic penumbra in a model of reversible middle cerebral artery occlusion in the rat. Experimental Brain Research. 1992; 89:67–78. [PubMed: 1601103]
36. Shih AY, Friedman B, Drew PJ, Tsai PS, Lyden PD, Kleinfeld D. Active dilation of penetrating arterioles restores red blood cell flux to penumbral neocortex after focal stroke. Journal of Cerebral Blood Flow & Metabolism. 2009; 29:738–751. [PubMed: 19174826]
37. Campbell BC, Christensen S, Tress BM, Churilov L, Desmond PM, Parsons MW, Barber PA, Levi CR, Bladin C, Donnan GA, Davis SM. Failure of collateral blood flow is associated with infarct growth in ischemic stroke. Journal of Cerebral Blood Flow & Metabolism. 2013; 33:1168–1172. [PubMed: 23652626]
38. Devor A, Hillman EM, Tian P, Waeber C, Teng IC, Ruvinskaya L, Shalinsky MH, Zhu H, Haslinger RH, Narayanan SN, Ulbert I, Dunn AK, Lo EH, Rosen BR, Dale AM, Kleinfeld D, Boas DA. Stimulus-induced changes in blood flow and 2-deoxyglucose uptake dissociate in ipsilateral somatosensory cortex. Journal of Neuroscience. 2008; 28:14347–14357. [PubMed: 19118167]
39. Drew PJ, Shih AY, Kleinfeld D. Fluctuating and sensory-induced vasodynamics in rodent cortex extends arteriole capacity. Proceedings of the National Academy of Sciences USA. 2011; 108:8473–8478.
40. Mayhew JEW, Askew S, Zeng Y, Porrill J, Westby GWM, Redgrave P, Rector DM, Harper RM. Cerebral vasomotion: 0.1 Hz oscillation in reflectance imaging of neural activity. Neuroimage. 1996; 4:183–193. [PubMed: 9345508]
41. Nelson MT, Patlak JB, Worley JF, Standen NB. Calcium channels, potassium channels, and voltage dependence of arterial smooth muscle tone. American Journal of Physiology. 1990; 259:C3–C18. [PubMed: 2164782]
42. Hudlická O, Zweifach BW, Tyler KR. Capillary recruitment and flow velocity in skeletal muscle after contractions. Microvascualr Researchla. 1982; 23:201–213.
43. Kim T, Kim SG. Temporal dynamics and spatial specificity of aterial and venous blood volume changes during visual stimulation: Implication for BOLD quantification. Journal of Cerebral Blood Flow & Metabolism. 2011; 31:1211–1222. [PubMed: 21179068]
44. Kleinfeld, D. Cortical blood flow through individual capillaries in rat vibrissa S1 cortex: Stimulus induced changes are comparable to underlying fluctuations in flow. In: Tomita, M., editor. Brain Activation and Cerebral Blood Flow Control. Elsevier International Congress Series; Tokyo: 2002.
45. Villringer A, Haberl RL, Dirnagl U, Anneser F, Verst M, Einhaupl KM. Confocal laser microscopy to study microcirculation on the rat brain surface *in vivo*. Brain Research. 1989; 504:159–160. [PubMed: 2598012]
46. Nishimura N, Schaffer CB, Friedman B, Tsai PS, Lyden PD, Kleinfeld D. Targeted insult to individual subsurface cortical blood vessels using ultrashort laser pulses: Three models of stroke. Nature Methods. 2006; 3:99–108. [PubMed: 16432519]

47. Shih AY, Blinder P, Tsai PS, Friedman B, Stanley G, Lyden PD, Kleinfeld D. The smallest stroke: Occlusion of one penetrating vessel leads to infarction and a cognitive deficit. Nature Neuroscience. 2013; 16:55–63.
48. Nishimura N, Rosidi NL, Iadecola C, Schaffer CB. Limitations of collateral flow after occlusion of a single cortical penetrating arteriole. Journal of Cerebral Blood Flow & Metabolism. 2010; 30:1914–1927. [PubMed: 20842163]
49. Nedergaard M, Hansen AJ. Characterization of cortical depolarizations evoked in focal cerebral ischemia. Journal of Cerebral Blood Flow & Metabolism. 1993; 13:658–574.
50. Grynkiewicz G, Poenie M, Tsien RY. A new generation of Ca^{2+} indicators with greatly improved fluorescence properties. Journal of Biological Chemistry. 1985; 260:3440–3450. [PubMed: 3838314]
51. Bederson JB, Pitts LH, Germano SM, Nishimura MC, Davis RL, Bartkowski HM. Evaluation of 2,3,5-triphenyltetrazolium chloride as a stain for detection and quantification of experimental cerebral infarction in rats. Stroke. 1986; 17:1304–1308. [PubMed: 2433817]
52. Drew PJ, Shih AY, Driscoll JD, Knutsen PM, Davalos D, Blinder P, Akassoglou K, Tsai PS, Kleinfeld D. Chronic optical access through a polished and reinforced thinned skull. Nature Methods. 2010; 7:981–984. [PubMed: 20966916]
53. Hutson KA, Masterton RB. The sensory contribution of a single vibrissa's cortical barrel. Journal of Neurophysiology. 1986; 56:1196–1223. [PubMed: 3783236]
54. Anenberg E, Arstikaitis P, Niitsu Y, Harrison TC, Boyd JD, Hilton BJ, Tetzlaff W, Murphy TH. Ministrokes in channelrhodopsin-2 transgenic mice reveal widespread deficits in motor output despite maintenance of cortical neuronal excitability. Journal of Neuroscience. 2014; 34:1094–1104. [PubMed: 24453302]
55. Pries AR, Secomb TW. Microvascular blood viscosity *in vivo* and the endothelial surface layer. American Journal of Physiology - Heart and Circulation Physiology. 2005; 289:H2657–2664.
56. Snodderly DM, Weinhaus RS, Choi JC. Neural-vascular relationships in central retina of macaque monkeys (Macaca fascicularis). Journal of Neuroscience. 1992; 12:1169–1193. [PubMed: 1556592]
57. Fox MD, Raichle ME. Spontaneous fluctuations in brain activity observed with functional magnetic resonance imaging. Nature Reviews of Neuroscience. 2007; 8:700–711.
58. Biswal B, Yetkin FZ, Haughton VM, Hyde JS. Functional connectivity in the motor cortex of resting human brain using echo-planar MRI. Magnetic Resonance in Medicine. 1995; 34:537–541. [PubMed: 8524021]
59. Vincent JL, Patel GH, Fox MD, Snyder AZ, Baker JT, Van Essen DC, Zempel JM, Snyder LH, Corbetta M, Raichle ME. Intrinsic functional architecture in the anaesthetized monkey brain. Nature. 2007; 447:83–88. [PubMed: 17476267]
60. Leopold DA, Murayama Y, Logothetis NK. Very slow activity fluctuations in monkey visual cortex: Implications for functional brain imaging. Cerebral Cortex. 2003; 13:422–433. [PubMed: 12631571]
61. Osol G, Halpern W. Spontaneous vasomotion in pressurized cerebral arteries from genetically hypertensive rats. American Journal of Physiology. 1988; 254:H28–H33. [PubMed: 3337256]
62. Aalkjaer C, Nilsson H. Vasomotion: cellular background for the oscillator and for the synchronization of smooth muscle cells. British Journal of Pharmacology. 2005; 144:605–616. [PubMed: 15678091]
63. Mateo, C.; Tsai, PS.; Shih, AY.; Kleinfeld, D. Society for Neurocience Annual Meeting. Society for Neurocience; San Diego: 2013. Probing neurovascular coupling via natural and driven vasomotion in the awake mouse.
64. Dore-Duffy P, Cleary K. Morphology and properties of pericytes. Methods in Molecular Biology. 2011; 686:49–68. [PubMed: 21082366]
65. Peppiatt CM, Howarth C, Mobbs P, Attwell D. Bidirectional control of CNS capillary diameter by pericytes. Nature. 2006; 443:642–643.
66. Hall CN, Reynell C, Gesslein B, Hamilton NB, Mishra A, Sutherland BA, O'Farrell FM, Buchan AM, Lauritzen M, Attwell D. Capillary pericytes regulate cerebral blood flow in health and disease. Nature. 2014; 508:55–60. [PubMed: 24670647]

67. Kelley C, D'Amore P, Hechtman HB, Shepro D. Vasoactive hormones and cAMP affect pericyte contraction and stress fibres *in vitro*. Journal of Muscle Research and Cell Motility. 1988; 9:184–194. [PubMed: 2458383]
68. Fernández-Klett F, Offenhauser N, Dirnagl U, Priller J, Lindauer U. Pericytes in capillaries are contractile *in vivo*, but arterioles mediate functional hyperemia in the mouse brain. Proceedings of the National Academy of Sciences USA. 2010; 107:22290–22295.
69. Bandopadhyay R, Orte C, Lawrenson JG, Reid AR, De Silva S, Allt G. Contractile proteins in pericytes at the blood-brain and blood-retinal barriers. Journal of Neurocytology. 2001; 30:35–44. [PubMed: 11577244]
70. Nehls V, Drenckhahn D. Heterogeneity of microvascular pericytes for smooth muscle type alpha-actin. Journal of Cell Biology. 1991; 113:147–154. [PubMed: 2007619]
71. Murfee WL, Skalak TC, Peirce SM. Differential arterial/venous expression of NG2 proteoglycan in perivascular cells along microvessels: Identifying a venule-specific phenotype. Microcirculation. 2005; 12:151–160. [PubMed: 15824037]
72. Zhu X, Bergles DE, Nishiyama A. NG2 cells generate both oligodendrocytes and gray matter astrocytes. Development. 2008; 135:145–157. [PubMed: 18045844]
73. Zhu X, Hill RA, Dietrich D, Komitova M, Suzuki R, Nishiyama A. Age-dependent fate and lineage restriction of single NG2 cells. Development. 2011; 138:745–753. [PubMed: 21266410]
74. Nehls V, Drenckhahn D. The versatility of microvascular pericytes: from mesenchyme to smooth muscle? Histochemistry. 1993; 99:1–12. [PubMed: 8468190]
75. Dymecki SM, Ray RS, Kim JC. Mapping cell fate and function using recombinase-base intersectional strategies. Methods in Enzymology. 2010; 477:183–213. [PubMed: 20699143]
76. Madisen L, Zwingman TA, Sunkin SM, Oh SW, A ZH, Gu H, Ng LL, Palmiter RD, Hawrylycz MJ, Jones AR, Lein ES. A robust and high-throughput Cre reporting and characterization system for the whole mouse brain. Nature Neuroscience. 2010; 13:133–140.
77. Vinters HV, Ellis WG, Zarow C, Zaias BW, Jagust WJ, Mack WJ, Chui HC. Neuropathologic substrates of ischemic vascular dementia. Journal of Neuropathology and Experimental Neurology. 2000; 59:931–945. [PubMed: 11089571]
78. van Veluw SJ, Zwanenburg JJ, Engelen-Lee J, Spliet WG, Hendrikse J, Luijten PR, Biessels GJ. *In vivo* detection of cerebral cortical microinfarcts with high-resolution 7T MRI. Journal of Cerebral Blood Flow & Metabolism. 2013; 33:322–329. [PubMed: 23250109]
79. van Dalen JW, Scuric EEM, van Veluw SJ, Caan MWA, Nederveen AJ, Biessels GJ, van Gool WA, Richard E. Cortical microinfarcts detected in vivo on 3 Tesla MRI clinical and radiological correlates. Stroke. 2015; 46:255–257. [PubMed: 25468879]
80. Smith EE, Schneider JA, Wardlaw JM, Greenberg SM. Cerebral microinfarcts: The invisible lesions. Lancet Neurology. 2012; 11:272–282.
81. Iadecola C. The pathobiology of vascular dementia. Neuron. 2013; 80:844–866. [PubMed: 24267647]
82. Jellinger KA. Pathology and pathogenesis of vascular cognitive impairment: A critical update. Frontiers in Aging Neuroscience. 2013; 5:17. [PubMed: 23596414]
83. Lipton SA. Pathologically activated therapeutics for neuroprotection. Nature Reviews of Neuroscience. 2007; 8:803–808.
84. Werring DJ, Gregoire SM, Cipolotti L. Cerebral microbleeds and vascular cognitive impairment. Journal of the Neurological Sciences. 2009; 299:131–135. [PubMed: 20850134]
85. Vernooij MW, van der Lugt A, Ikram MA, Wielopolski PA, Niessen WJ, Hofman A, Krestin GP, Breteler MM. Prevalence and risk factors of cerebral microbleeds: The Rotterdam Scan Study. Neurology. 2008; 70:1208–1214. [PubMed: 18378884]
86. Poels MM, Vernooij MW, Ikram MA, Hofman A, Krestin GP, van der Lugt A, Breteler MM. Prevalence and risk factors of cerebral microbleeds: An update of the Rotterdam scan study. Stroke. 2010; 41:S103–S106. [PubMed: 20876479]
87. Nishimura N, Schaffer CB. Big effects from tiny vessels: Imaging the impact of microvascular clots and hemorrhages on the brain. Stroke. 2013; 44:S90. [PubMed: 23709743]

88. Rosidi NL, Zhou J, Pattanaik S, Wang P, Jin W, Brophy M, Olbricht WL, Nishimura N, Schaffer CB. Cortical microhemorrhages cause local inflammation but do not trigger widespread dendrite degeneration. Public Library of Science ONE. 2011; 6:e26612. [PubMed: 22028924]

89. Cianchetti A, Kim DK, Dimiduk S, Nishimura N, Schaffer CB. Stimulus-evoked calcium transients in somatosensory cortex are temporarily inhibited by a nearby microhemorrhage. Public Library of Science: ONE. 2013; 8:e65663. [PubMed: 23724147]

90. Matute C, Domercq M, Pérez-Samartín A, Ransom BR. Protecting white matter from stroke injury. Stroke. 2013; 44:1204–1211. [PubMed: 23212168]

91. Muller A, Joseph V, Slesinger PA, Kleinfeld D. Cell-based reporters reveal in vivo dynamics of dopamine and norepinephrin release in murine cortex. Nature Methods. 2014; 11:1245–1252. [PubMed: 25344639]

92. Hartmann DA, Underly RG, Watson AN, Shih AY. A murine toolbox for imaging the neurovascular unit. Microcirculation. 2014 Epub ahead of print.

93. Ding JB, Takasaki KT, Sabatini BL. Supraresolution imaging in brain slices using stimulated-emission depletion two-photon laser scanning microscopy. Neuron. 2009; 63:429–437. [PubMed: 19709626]

94. Kobat D, Durst ME, Nishimura N, Wong AW, Schaffer CB, Xu C. Deep tissue multiphoton microscopy using longer wavelength excitation. Optics Express. 2009; 17:13354–13364. [PubMed: 19654740]

95. Horton NG, Wang K, Kobat D, Clark CG, Wise FW, Schaffer CB, Xu C. *In vivo* three-photon microscopy of subcortical structures within an intact mouse brain. Nature Photonics. 2013; 7 10.1038/nphoton.2012.336.

96. Sofroniew MV, Vinters HV. Astrocytes: Biology and pathology. Acta Neuropathology. 2010; 119:7–35.

97. Brundel M, de Bresser J, van Dillen JJ, Kappelle LJ, Biessels GJ. Cerebral microinfarcts: A systematic review of neuropathological studies. Journal of Cerebral Blood Flow & Metabolism. 2012; 32:425–436. [PubMed: 22234334]

98. De Reuck J, Deramecourt V, Cordonnier C, Leys D, Pasquier F, Maurage CA. Prevalence of small cerebral bleeds in patients with a neurodegenerative dementia: A neuropathological study. Journal of the Neurological Sciences. 2011; 300:63–66. [PubMed: 20965516]

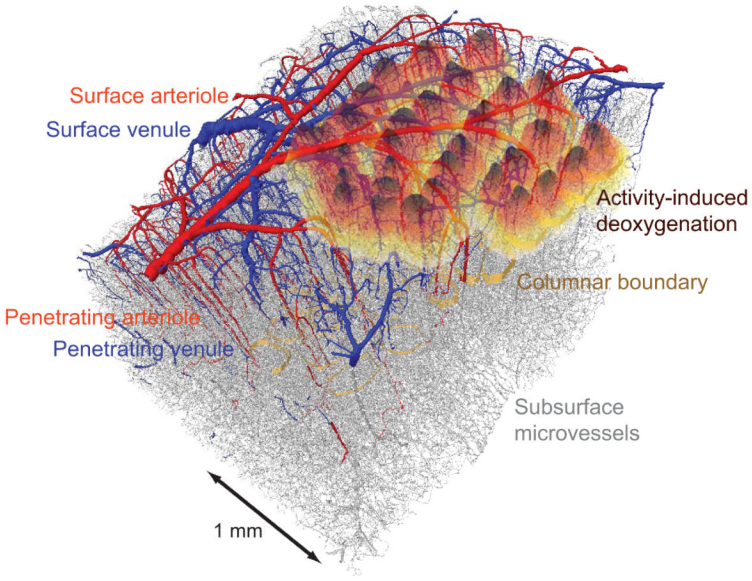

Figure 1. A vectorized data set of all vasculature in a block of parietal cortex that encompasses the primary vibrissa representation

The block is 2 mm by 3 mm by 1.2 mm thick. Surface and penetrating arterioles are colored red, venules blue, and the borders of cortical columns denoted by a golden band. A map of brain activity is superimposed. It was obtained from the contralateral hemisphere using intrinsic optical signal through a thinned-skull window. The animals were anesthetized with isoflurane so that only a net deoxyhemoglobin signal is observed by reflectance of 625 - nm light when individual vibrissae were deflected at 10 Hz for 4 s. The responses from all columns were normalized in amplitude and thresholded to avoid spatial overlap, and are superimposed on the vectorized data set. This new data was obtained using the methodology in Blinder *et al.* [17].

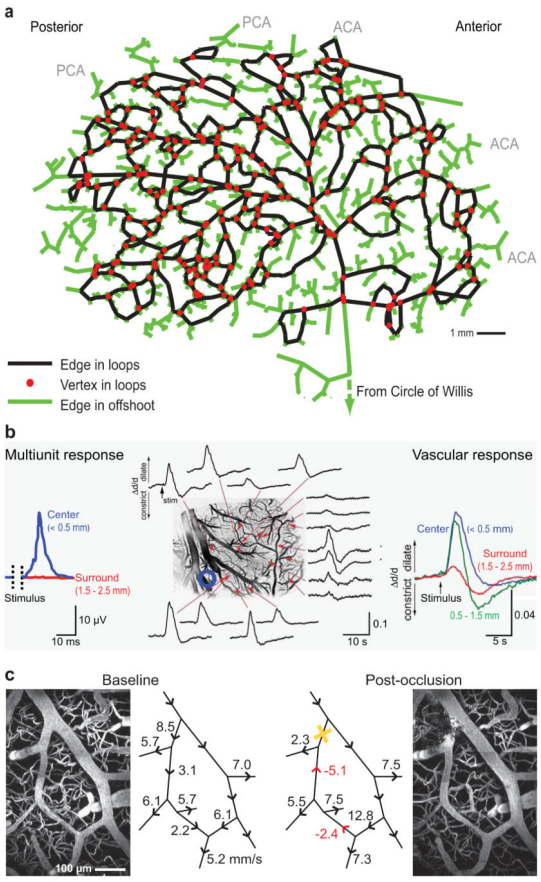

Figure 2. The pial surface forms a two dimensional network

(a) Representative example of a complete tracing of the vasculature fed by the middle cerebral artery. Parts that form loops are highlighted with black edges and red vertices, while non-backbone offshoots are shown in green. Adapted from Blinder *et al.* [21]. **(b)**. Stimulation of the footpad in the urethane anesthetized rat leads to local dilation but surrounding constriction of surface arterioles. Data in the left panel shows the evoked neuronal response, using ball electrode measurements of surface potentials, from nine different locations are shown. The strongest amplitude and fastest rise time was marked as the center of the receptive field. The middle panel shows a vascular map with the center of the receptive filed marked by a blue circle and arteriolar diameter change as a function of time and distance from the center. All data is shown as a fractional change relative to the baseline, *i.e.*, Δd/d, and dilation and constriction are plotted upward and downward respectively. The right panel is an average of arteriolar diameter changes within 0.5 mm from the center of neuronal response (blue), in a 0.5 - 1.5 mm annulus around the center (green) and 1.5 - 2.5 mm ring around the center (red) for all data from this animal. Adapted from Devor *et al.* [28]. **(c)**. Occlusion to a single surface arteriole leads to reversal of flow in the immediate downstream vessel and mild adjustment of flow in all branches. Data from rat anesthetized with urethane. On the left and right are *in vivo* two-photon images taken before and after photo-thrombotic clotting of an individual vessel, respectively. Left-center and right-center are diagrams of the surface vasculature with RBC speeds and directions

indicated. The yellow “X” indicates the location of the clot, and vessels whose flow direction has reversed are indicated with red arrows. Adapter from Schaffer *et al.* [33].

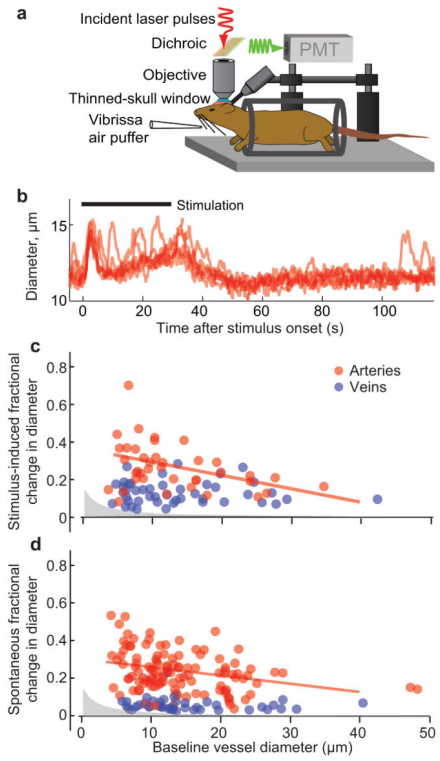

Figure 3. Stimulus driven and spontaneous vascular dynamics in the cortex of awake mice have similar amplitudes

(a) Schematic of the experimental setup. The awake mouse is head-fixed by means of a bolt and sits passively in an acrylic cylinder beneath the two-photon microscope. Air puffers for sensory stimulation are aimed at the vibrissa and, as a control, at the tail. **(b)** Example of evoked and spontaneous diameter change for a 30 s stimulus. **(c, d)** Relationship between peak value of the dilation and vessel diameter. Data for arteries is in red and for veins is in blue. Grey area shows the 0.2-µm resolution limit of detectable changes. Panel c shows the peak averaged dilation responses in the first 1 to 10 s of a 30 s vibrissae stimulation; the regression line has a statistically significant slope of −0.007/µm. Panel d shows the peak of spontaneous dilation; the regression line has a statistically significant slope of −0.004/µm. The regression for veins (not shown) is not significantly different from zero in either case. Adapted from Drew *et al.* [39].

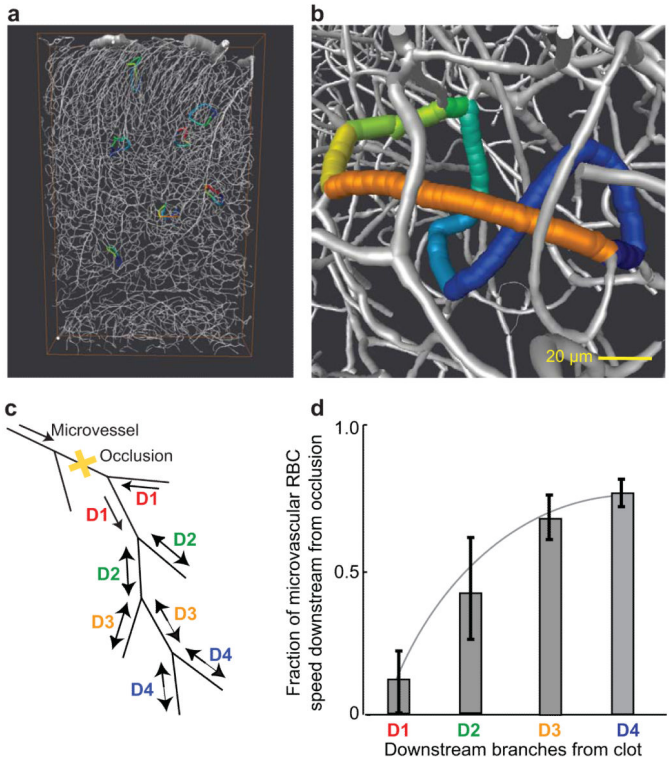

Figure 4. The subsurface microvasculature forms a three dimensional network that is largely insensitive to occlusion in one microvessel

(a) Numerical section of a vectorized network from a complete reconstruction (Figure 1). **(b)** Close up of the section in panel a showing only the microvasculature. The colored edges highlight a loop that consists of eight branches, each with a distinct color. Panels a and b adapted from Blinder *et al.* [17]. **(c)** Schematic of the microvasculature labeled with the order of downstream vessels, *i.e.*, D1 through D4 in this picture, from a point of occlusion. **(d)** The fraction of speed in downstream microvessels after an occlusion, yellow "X" in panel c, relative to that before the occlusion. The data is averaged over twenty networks in terms of downstream branch number. Panels c and d adapted from Nishimura *et al.* [46].

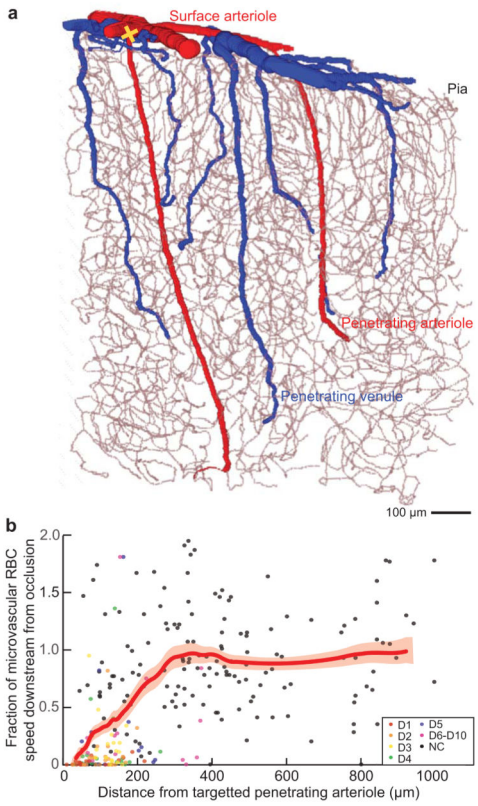

Figure 5. The penetrating arterioles are a fragile link in the delivery of blood from the surface arterioles to the subsurface microvascular network

(a) Numerical section of a vectorized network from a complete reconstruction (Figure. 1) that highlights the penetrating arterioles (red) and venules (blue) and the continuous microvascular network (gray). Adapted from Blinder *et al.* [17]. **(b)** The fraction of speed in neighboring microvessels that lie in cortical layers 2/3 after an occlusion to a single microvessel, relative to that before the occlusion. Only some of the data points could be specified in terms of downstream branch number, as shown. The thick red line through the data is the smoothed response averaged over a window that included 50 points, with ± 1 SEM limits indicated by the thin red lines. The data is averaged over 16 networks. Adapted from Nishimura *et al.* [23].

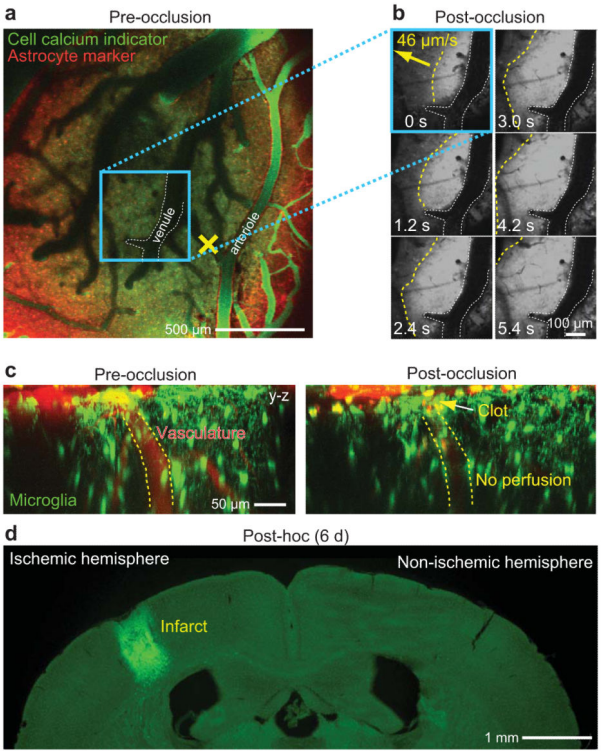

Figure 6. Occlusion to one penetrating arteriole results in neuronal death and formation of a cyst

(a) *In vivo* two-photon imaging of neuronal activity in the forelimb region of somatosensory cortex of an α-chloralose anesthetized rat that was loaded with the [Ca^{2+}] indicator OGB1-AM and the astrocyte-specific dye SR101. The single penetrating arteriole marked by a yellow "X" was occluded. **(b)** Wave of cortical spreading depression, propagating at 46 μm/s, observed by *in vivo* [Ca^{2+}] imaging (yellow dashed line) about 30 minutes after occlusion of the penetrating arteriole (yellow arrow, left). Panels a and b adapted from Shih *et al.* [47]. **(c)** Maximal projection through a 200-μm depth of a *Cx3cr1*$^{eGFP/+}$ mouse cortex before (left) and 100 minutes after (right) occlusion of a single penetrating arteriole using targeted optical activation of the photothrombotic agent Rose Bengal (arrow) made 1 day after implantation of a transcranial window [52]. Dashed lines indicate the boundaries of the penetrating artery in which flow was blocked (yellow "X"). (**d**) Extent of the infarct, for the same mouse as in panel c, visualized 2 day after the optically generated stroke. The bright green fluorescence indicates the invasion of eGFP-labeled microglia into a cyst of necrotic tissue. Adapted from Drew *et al.* [52].

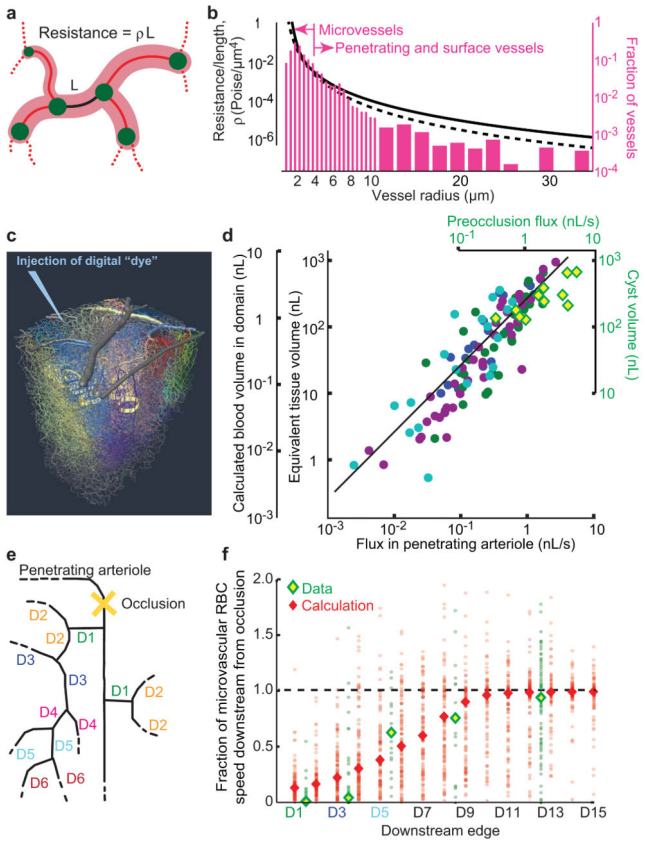

Figure 7. The calculated pattern of blood flow for a full reconstruction of the vasculature (Figure 1) accounts for the measured degradation in flow after blocking a single penetrating arteriole

(a) Reduction of the angioarchitecture to vertices (green dots) and branches (red). The resistance of each branch depends on the radius and length, L. (**b**) Plot of the flow resistance,ρ, per unit length as a function of vessel radius (solid curve); the total resistance is found by multiplying ρ by the length, in micrometers. Note the marked increase in resistance for radii below ~ 5 μm. The Hagen-Poiseuille law is given by the dashed curve. The concurrent histogram shows the distribution of vessel radii for all vessels. **(c)** Vectorized vasculature in which the blood flow through a single penetrating arteriole is numerically labeled to determine the spatial domain of vessels that receive at least half of their flow from the chosen penetrating arteriole. This exercise is repeated for all penetrating arterioles and each domain is additionally labeled by the flux through the penetrating vessel. **(d)** Plot of the computed vascular perfusion domains versus flux in the penetrating arteriole. The volume of the parenchymal domains (115 domains in 4 data sets; colored circles) are consistent with measured cyst volumes formed after a single artery occlusion (11 rats). (**e**) Schematic of the microvasculature labeled with the order of downstream vessels, *i.e.*, D1 through D4 in this picture, from a point of occlusion of an individual penetrating arteriole. **(f)** The calculated redistribution of flow in microvessels, up to 15 edges downstream from the sites of simulated occlusion of selected, individual penetrating arterioles. The reduction in vascular flux is plotted as a function of the order of the downstream vessel (red circles are the results of 100 simulations per order of the downstream edge and red diamonds are the median reduction in flux). These numerical results are compared with the published *in vivo* data of

downstream flux measurement before and after penetrating arteriole occlusion in rat neocortex (green points are data from 175 vessels with median values shown as yellow and green diamonds). All panels adapted from [17].

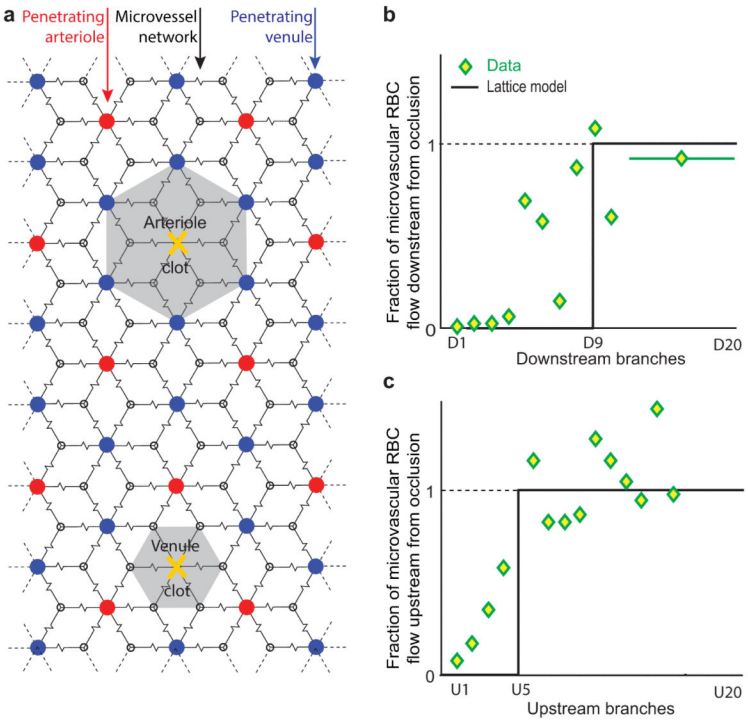

Figure 8. A two-dimensional lattice model of the vasculature that approximates the measured degradation in flow after blocking a single penetrating arteriole

(a) Planar circuit with a rhombic lattice and two penetrating venules for each penetrating arteriole, consistent with measurements of actual penetrating arteriole vs. ascending venule densities.. Blockage of a penetrating arteriole leads to a region of no flow with an effective radius of 0.9-times the median spacing between penetrating venules, whereas blockage of a penetrating venule leads to a region of no flow with an effective radius of 0.5-times the median spacing between penetrating venules. Adapted from Blinder *et al.* [17]. **(b)** Comparison of the prediction from the lattice model and data for flow in downstream microvessels after blockage to a penetrating arteriole. Adapted from Nishimura *et al.* [48] and Blinder *et al.* [17]. **(c)** Comparison of the prediction from the lattice model and data for flow in upstream microvessels after blockage to a penetrating venule. Adapted from Nguyen *et al.* [25] and Blinder *et al.* [17].

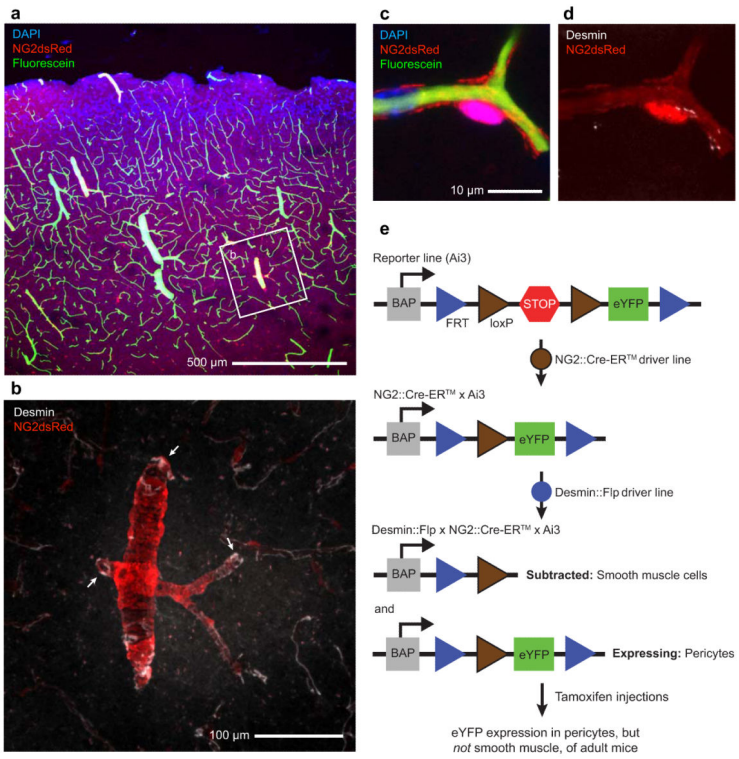

Figure 9. Pericytes are a potential means for the brain to control its own blood supply

The data are maximum projections though stacks of confocal images from a transgenic mouse brain that expressed NG2::dsRed (red), *i.e.*, the fluorescent protein dsRed is linked to expression of NG2 [72]. The animal was perfused with a fluorescein-labeled albumin gelatin [1] (green) and sections were labeled with α-desmin antibody (white) and stained for DAPI (blue) to identify cell nuclei. **(a)** Overview with areas noted for detailed analysis. Projection across 37 sections in 1.05 µm steps. The fluorescein channel is saturated and desmin channel is excluded. **(b)** Illustration of a penetration arteriole, with staining for both NG2 and desmin (arrows point to expression at cuts through lumen) other channels are excluded. Projection across 43 sections in 1.0 µm steps. **(c, d)** High magnification view of microvessels and, presumably, pericytes with lack of labeling for desmin. Projection is across 32 sections in 1.0 µm steps. **(e)** Proposed dual-recombinase strategy to form a transgenic animal that labels pericytes but not smooth muscle. We cross the Ai3 reporter mouse [76] (Jax: 007903) with the tamoxifen-indicable NG2::CreER^{TM} driver mouse [73] (Jax: 008538), and then a hypothetical desmin::Flp driver mouse. The expressing cells should be pericyte, as indicated, as well as oligodendrocyte precursors and sparse labeled neurons. “BAP” stands for the broadly active promoter plus a set of cis-regulatory sequences and “eYFP” for enhanced yellow fluorescent protein.

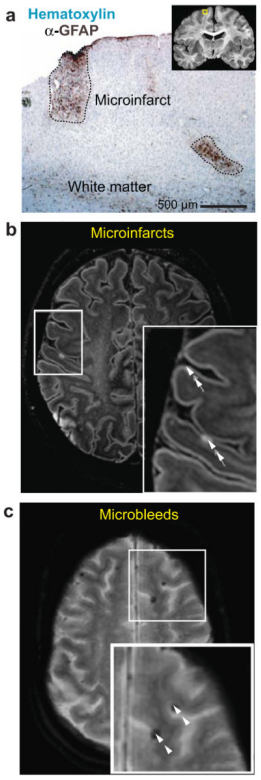

Figure 10. Neuropathological evidence of "invisible" lesions in the aging human brain

(a) Example of gray matter microinfarcts in a light-level microscopy neuropathological study by Sofroniew and Vinters [96]. **(b)** Detection of cerebral microinfarcts with fluid attenuation inversion recovery (FLAIR) magnetic resonance imaging (MRI) at 7 Tesla. Adapted from Brundel *et al.* [97]. **(c)** Detection of cerebral microbleeds with T2* gradient echo MRI at 3T. Adapted from De Reuck *et al.* [98].